A dike–groyne algorithm in a terrain-following coordinate ocean model (FVCOM): Development, validation and application

Jianzhong Ge [a,*], Changsheng Chen [a,b], Jianhua Qi [b], Pingxing Ding [a], Robert C. Beardsley [c]

[a] State Key Laboratory for Estuarine and Coastal Research, East China Normal University, 200062 Shanghai, PR China
[b] School for Marine Science and Technology, University of Massachusetts-Dartmouth, New Bedford, MA 02744, USA
[c] Department of Physical Oceanography, Woods Hole Oceanographic Institution, Woods Hole, MA 02543, USA

ABSTRACT

A dike–groyne module is developed and implemented into the unstructured-grid, three-dimensional primitive equation finite-volume coastal ocean model (FVCOM) for the study of the hydrodynamics around human-made construction in the coastal area. The unstructured-grid finite-volume flux discrete algorithm makes this module capable of realistically including narrow-width dikes and groynes with free exchange in the upper column and solid blocking in the lower column in a terrain-following coordinate system. This algorithm used in the module is validated for idealized cases with emerged and/or submerged dikes and a coastal seawall where either analytical solutions or laboratory experiments are available for comparison. As an example, this module is applied to the Changjiang Estuary where a dike–groyne structure was constructed in the Deep Waterway channel in the inner shelf of the East China Sea (ECS). Driven by the same forcing under given initial and boundary conditions, a comparison was made for model-predicted flow and salinity via observations between dike–groyne and bed-conforming slope algorithms. The results show that with realistic resolution of water transport above and below the dike–groyne structures, the new method provides more accurate results. FVCOM with this MPI-architecture parallelized dike–groyne module provides a new tool for ocean engineering and inundation applications in coastal regions with dike, seawall and/or dam structures.

© 2012 Elsevier Ltd. All rights reserved.

1. Introduction

It is a challenge for a terrain-following coordinate coastal ocean model to simulate the flow field in an estuarine or coastal system with dikes and groynes. The constructions are usually submerged during high tide but may be fully exposed during low tide. If they are treated as submerged vertical walls, the terrain-following coordinate transformation cannot be directly applied. Adding a slope on the surface of a dike or groyne could make the topographic coordinate transformation work (e.g. Qi, 2003; Du, 2007), but it changes the hydrodynamics. Instead of solid blocking (no flux towards the wall) in the lower column with the dike or groyne and free exchange in the upper column above the construction, that type of construction makes the water tend to flow along the submerged part under the dynamical constraints of the sloping bottom boundary layer. As a result, this approach can overestimate vertical and lateral mixing and thus produce unrealistic circulation around the construction.

Recently, inundation has received intense attention for model applications to coastal and estuarine problems. It is defined as coastal flooding of normally dry land caused by heavy rains, high river discharge, tides, storm surge, tsunami processes, or some combination thereof. In many coastal regions, dams are built around the area where the height of land is lower or close to the mean sea level to protect the land from flooding (Pullen et al., 2007, 2008, 2009; Lhomme et al., 2008; Allsop et al., 2009). An coastal inundation forecast system is aimed at (1) making warming of coastal flooding on an event timescale in order to facilitate evacuation and other emergency measures to protect human life and property and (2) estimating accurate statistics of coastal inundation in order to enable rational planning regarding sustainable land-use practices in the coastal zone. A model used for this application must produce accurate, real-time forecasts of water level at high spatial resolution in the coastal zone and have the capability to resolve the overtopping process of dams and similar structures. These dams are like a solid wall boundary when the water level is lower than it, but become submerged constructions like dikes when flooding occurs. The existing wet/dry treatment technology available in current terrain-following coordinate system models (e.g. Lynch and Gray, 1980; Johns et al., 1982; Zheng et al., 2003; Chen et al., 2007; Zhao et al., 2010) is capable of resolving coastal

* Corresponding author. Tel.: +86 21 62232495.
  E-mail addresses: gegsdw@hotmail.com, jzge@sklec.ecnu.edu.cn (J. Ge), c1chen@umassd.edu (C. Chen), jqi@umassd.edu (J. Qi), pxding@sklec.ecnu.edu.cn (P. Ding), rbeardsley@whoi.edu (R.C. Beardsley).

flooding in many situations but not those with vertical seawalls in the computational domain. It is imperative that we implement a dike–groyne treatment module in a terrain-following coordinate unstructured-grid coastal ocean numerical model if we are to apply this type of model to accurately simulate the complex flow fields found in coastal and estuarine regions with submerged dikes and groynes.

There have been many efforts on examining the fluid flow features in the dike and groyne systems and developing discrete algorithms to resolve these features in real applications (Ouillon and Dartus, 1997; Muto et al., 2002; Uijttewaal, 2005; Yossef, 2005; McCoy et al., 2006, 2007, 2008; Tang et al., 2006; Kurzke et al., 2002; Yeo and Kang, 2008; Uijttewaal et al., 2001; Yossef and Vriend, 2011; Delft3D-FLOW User Manual, 2009). Recent laboratory experiments revealed that the flow field between dikes is characterized by various types of eddies with significantly different spatial scales and fluctuations under conditions of submerged and emerged dikes (Yossef and Vriend, 2011). The fluid dynamics that control eddy formation and evolution were examined using Large Eddy Simulation (LES) (McCoy et al., 2006, 2007, 2008; Tang et al., 2006; Ouillon and Dartus, 1997). A Computational Fluid Dynamics (CFD) program (named FLOW-3D) was developed to simulate the flow structures around a submerged groyne (Yeo and Kang, 2008). This program, however, is designed for the CFD scale without consideration of the earth's rotation. In order to apply this program to realistic ocean situations, the program must be couple with an ocean model. The Delft3D-FLOW (Delft3D-FLOW User Manual, 2009) is the current commercial consulting software that is widely used for coastal and estuarine engineering. This model includes a dam treatment algorithm, which treats a dam as an infinitely thin object on a grid line. On this line, no water exchange between two computational cells connected to that line is allowed. This algorithm works well for Delft3D-FLOW, but the structured grids used in this model limits its application to resolve complex and irregular geometry of coastal ocean and estuaries.

A joint research team of the University of Massachusetts Dartmouth (UMassD) and Woods Hole Oceanographic Institution (WHOI) has developed the unstructured-grid, three-dimensional, primitive equations finite-volume coastal ocean model (FVCOM) (Chen et al., 2003, 2006a,b, 2007; Huang et al., 2008). FVCOM uses a non-overlapped triangular mesh in the horizontal and a terrain-following coordinate in the vertical. The triangular mesh used in FVCOM can resolve the geometry of dikes-groynes. With the wet/dry point treatment in this model, FVCOM is capable of predicting the water exchange over a dam on land. As with all other terrain-following coordinate models, however, FVCOM has an issue with including the correct kinematics for the case with submarine dikes-groynes.

In this paper, we have introduced an unstructured-grid algorithm to calculate the water velocity and tracer concentration in a dike–groyne system. This algorithm has been coded into FVCOM with MPI parallelization (Chen et al., 2006a; Cowles, 2008) and validated for idealized channel cases with dike–groyne construction where analytical solutions and laboratory experiment results are available for comparison and an idealized estuary with dike–groyne features. As an example of an application, we applied this algorithm to the Changjiang River (CR) for the simulation of the tidal and residual flows inside and outside of the dike–groyne system constructed there in the last decade.

The rest of the paper is organized as follows. In Section 2, an unstructured-grid discrete algorithm for the dike–groyne treatment is described. In Section 3, three idealized cases were selected to validate the dike–groyne module code under physical conditions driven by river discharge and tides and the overtopping process of a seawall. In Section 4, FVCOM with this new dike–groyne module is applied to the CR and validated with field measurement data, the

simulation results are presented, and the computational efficiency of the method is discussed. Conclusions are then summarized in Section 5.

2. An unstructured-grid dike–groyne algorithm

Three types of dike and groyne are considered: (a) "straight," (b) "joint" and (c) "cross" (Fig. 1). In plan view, the first is constructed by a straight line running along edges of triangles. The second consists of two lines, with the end point of one line connecting to the other line. The third is composed of two lines, with one crossing the other. In the vertical, we consider three different cases. In the first case, the tops of the structures are always below sea level. For this case, the water column connected to the structure is characterized by two layers: an upper layer in which the water can flow freely across the structure, and a lower layer in which flow is blocked (with no flux into the wall). In a free-surface model, due to the temporal variation of the surface elevation, the top of a dike or a groyne is probably contained within a terrain-following layer. For simplification, we define the interface of free and blocked layers either at the upper level (when a portion of the length of the structure is longer than half the thickness of the terrain-following layer) or at the lower level (when a portion of the length of the structure is shorter than half the thickness of the terrain-following layer). In the second case, the dikes and groynes are always above sea level. This is the simplest case in which the dikes and groynes can be easily treated as solid lateral boundaries. In the third case, the dikes and groynes are sometimes above and sometimes below sea level. For this case, the approaches used for the first and second cases are combined.

In general, the width of a dike or groyne is on the order of 2–5 m. For a numerical simulation with a horizontal resolution of > 20–100 m, these dikes or groynes can be treated as lines without width. Under this assumption, we can construct the triangular grid along dikes and groynes, with a single control volume above the structure and two separate control volumes beneath it (Fig. 2). The algorithm of the dike–groyne treatment is described as follows. An example is given for the algorithm used for a single dike or groyne, and this approach is simply extended for the case of multiple dikes and groynes.

2.1. Free-surface elevation

In the Cartesian coordinate system, the vertically integrated continuity equation can be written in the form of

$$\frac{\partial \zeta}{\partial t} = -\frac{1}{\Omega}\left[\oint_{l_\Omega}(\bar{u}D)\,\mathrm{d}y - \oint_{l_\Omega}(\bar{v}D)\,\mathrm{d}x\right] \tag{1}$$

where ζ is the free-surface elevation, u and v are the x- and y-components of the horizontal velocity, D is the total water depth defined
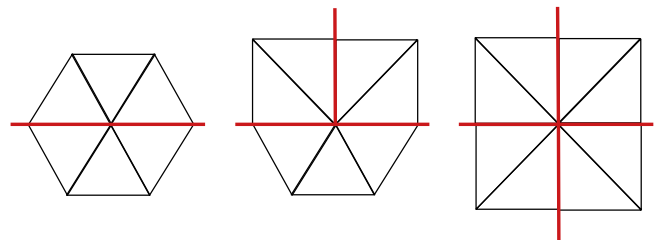
Fig. 1. Three types of dike and groyne construction. Type 1: a straight dike (left panel). Type 2: a groyne joined at its end with a dike (middle panel). Type 3: a groyne crossed through a dike (right panel). A horizontal red line indicates a dike and a vertical red line represents a groyne. The black lines are the triangle's edges. (For interpretation of the references to color in this figure legend, the reader is referred to the web version of this article.)
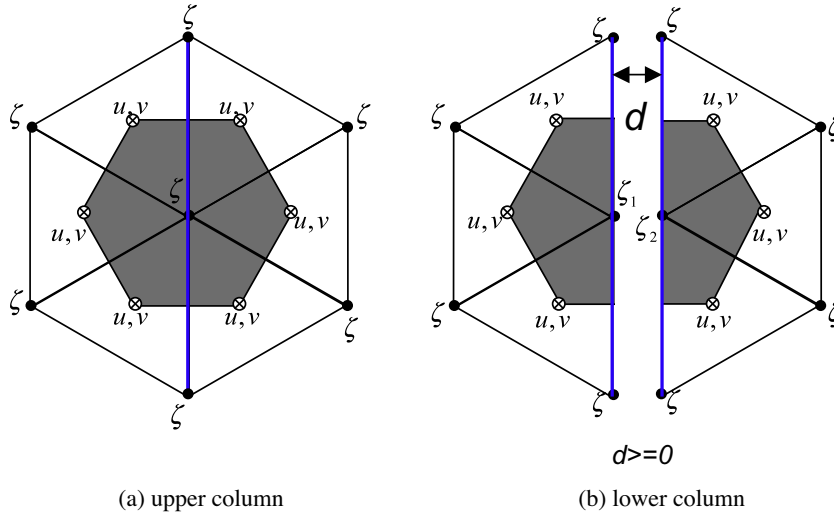
Fig. 2. Sketch of the separation of the control element at dikes or groynes. The shaded regions indicate the tracer control elements (TCEs).

as $H+\zeta$, and H is the mean water depth. In FVCOM, an unstructured triangle is comprised of three nodes, a centroid, and three sides, on which u and v are placed at centroids and all scalars (i.e., , H, D) are placed at nodes. u and v at centroids are calculated based on the net flux through the three sides of that triangle (shaded regions in Fig. 4, hereafter referred to as the Momentum Control Element: MCE), while scalar variables at each node are determined by the net flux through the sections linked to centroids and the middle point of the sideline in the surrounding triangles (shaded regions in Fig. 2), hereafter referred to as the Tracer Control Element: TCE). Ω is the area of the TCE.

Defining h as the height of dike or groyne, we divide a TCE into two elements (Fig. 2), calculate the fluxes individually, and then combine them. Applying (1) to each element, we have

$$\Omega_l \frac{\partial \zeta_l}{\partial t} = -\left[\int_{l_l} \bar{u}D dy - \int_{l_l} \bar{v}D dx\right] - \left[\int_{l_w} \bar{u}_w D dy - \int_{l_w} \bar{v}_w D dx\right] \quad (2)$$

$$\Omega_r \frac{\partial \zeta_r}{\partial t} = -\left[\int_{l_r} \bar{u}D dy - \int_{l_r} \bar{v}D dx\right] + \left[\int_{l_w} \bar{u}_w D dy - \int_{l_w} \bar{v}_w D dx\right] \quad (3)$$

where Ω_l and Ω_r are the areas of the two elements (hereafter referred to as left and right elements); l_w is the length of the element edge connected to the solid wall; l_l and l_r are the lengths of left and right elements (minus l_w); ζ_l and ζ_r are the surface elevations calculated by the flux derived from the left and right elements; u_w and v_w are the x- and y-components of the horizontal velocity at the edge of the element connected to the wall. u_w and v_w satisfy the boundary condition of no flux normal to the wall. Eqs. (2) and (3) are numerically solved using the modified fourth-order Runge–Kutta time-stepping scheme, the same as that used in FVCOM (Chen et al., 2003, 2006a).

For the case in which the dikes and groynes remain under the sea surface, adding (2) and (3) yields

$$\Omega_l \frac{\partial \zeta_l}{\partial t} + \Omega_r \frac{\partial \zeta_r}{\partial t} = -\left[\int_{l_l+l_r} \bar{u}D dy - \int_{l_l+l_r} \bar{v}D dx\right] \quad (4)$$

According to volume conservation, we can determine ζ at the node on the wall with a solution given as

$$\zeta = \frac{\Omega_l \zeta_l + \Omega_r \zeta_r}{\Omega_l + \Omega_r} \quad (5)$$

Eq. (5) is derived for a submerged dike or groyne case. For the case in which dikes and groynes are initially above sea level, the surface

elevation on either side of the wall is determined by ζ_l and ζ_r in (2) and (3). When the total water depth D on both sides is higher than the height of the wall, the surface elevation can be calculated by (5). When the total water depth on one side is higher than the height of the wall but on the other side is not, then the volume of the water above the height of the wall will move to the other side as a lateral flux. For example, assuming that the water on the left side, but not on the right side, is higher than the height of the wall (Fig. 3), i.e.,

$$D_l = H + \zeta_l > h; \qquad D_r = H + \zeta_r < h,$$

then the new surface elevations on the respective sides should be equal to

$$\hat{\zeta}_r = \zeta_r + \Delta\zeta_l \frac{\Omega_l}{\Omega_r} \text{ and } \hat{\zeta}_r = \zeta_l - \Delta\zeta_l \quad (6)$$

If the adjusted total water depth $D_r = H + \hat{\zeta}_r > h$, then a revised adjustment is made until ζ_l equals ζ_r. This approach is also applied to the case where the mean depths on opposite sides of the wall are different.

2.2. Horizontal and vertical velocities

In FVCOM, the horizontal velocity is calculated using the second-order upwind scheme derived by Kobayashi et al. (1999). This method was described in detail in Chen et al. (2003). When the dikes and groynes remain above sea level, then they are treated as a solid lateral boundary, and velocity at the centroid of a triangle connected to the wall can be easily determined using the same boundary treatment as in FVCOM (Chen et al., 2006a). For the case in which the dikes and groynes are below sea level, the velocity in the upper free-exchange ($-H + h \leq z \leq 0$) and lower solid-blocking
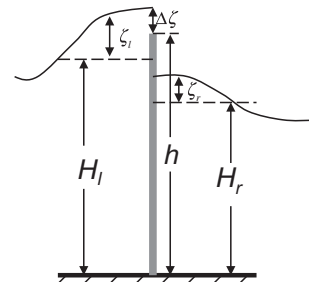
Fig. 3. Illustration of the treatment of the water exchange across a dike or a groyne when the water on either side is over the height of the construction.
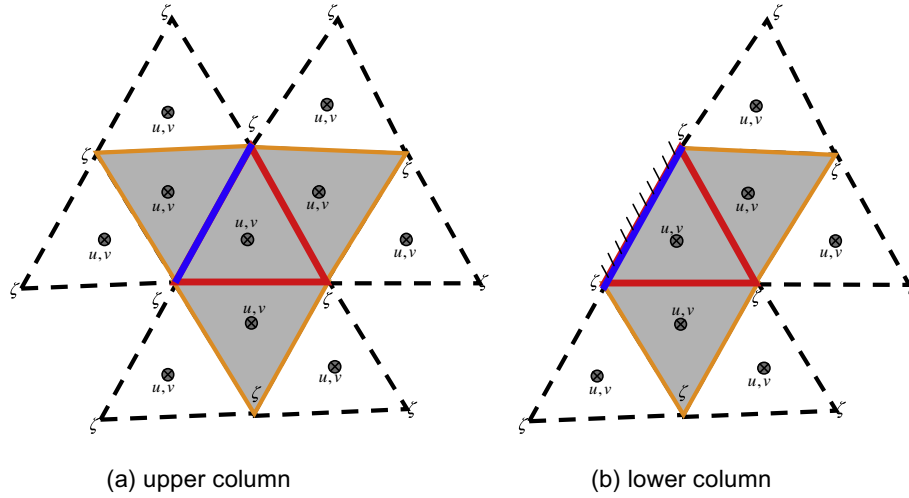
Fig. 4. Illustration of momentum control elements (shaded regions) used to calculate the horizontal velocity in the upper (above the height of the construction) and lower (below the height of the construction) layers.

$(-H \leq z < -H + h)$ layers are calculated based on the MCEs shown in Fig. 4a and b), respectively. No flux normal to the wall is applied to the MCE in the lower layer.

The governing equations in FVCOM are solved using either a semi-implicit scheme or a mode-split scheme. In the semi-implicit scheme, the velocity can be solved using the approach described here. In the mode-split scheme, the total water flux toward the wall equals $(D - h)\bar{v}_n$, where $\bar{v}_n$ is the component of vertically averaged velocity normal to the wall. This amount of transport must be considered in the 2-D mode to be consistent with the 3-D calculation.

The vertical velocity (ω) in the terrain-following vertical coordinate is calculated based on the same TCEs as those used for the surface elevation. In the upper free-exchange layer, ω is calculated using the combined TCE shown in Fig. 2a, i.e.,

$$\omega_{i,k+1} = \omega_{i,k} + \frac{\Delta\sigma_k}{\Delta t_i}(\zeta_i^{n+1} - \zeta_i^n) + \frac{\Delta\sigma_k}{\Omega_l + \Omega_r}\oint_{l_l + l_r} u_{N,k}^n D dl. \tag{7}$$

In the lower solid-blocked layer, ω at the vertical level in the left and right TCEs shown in Fig. 2b are calculated separately, as,

$$\begin{cases} \omega_{i,k+1}^l = \omega_{i,k}^l + \frac{\Delta\sigma_k}{\Delta t_i}(\zeta_i^{l,n+1} - \zeta_i^{l,n}) + \frac{\Delta\sigma_k}{\Omega_l}\oint_{l_l} u_{N,k}^n D \, dl \\ \omega_{i,k+1}^r = \omega_{i,k}^r + \frac{\Delta\sigma_k}{\Delta t_i}(\zeta_i^{r,n+1} - \zeta_i^{r,n}) + \frac{\Delta\sigma_k}{\Omega_r}\oint_{l_r} u_{N,k}^n D \, dl \end{cases} \tag{8}$$

where ω^l and ω^r are the vertical velocities at the separate left and right TCEs; k is the vertical level index.

2.3. Scalar variables (temperature, salinity, sediment concentration)

The calculation of scalar variables at nodes with triangles connected to dikes and groynes is similar to that used for the surface elevation and vertical velocity. A special treatment is made for the case in which the water is moved from one side (where the total water depth is greater than the height of the wall) to the other side (where the total water depth is less than the height of the wall). For example, in the case indicated in (6), $\Delta\zeta_l\Omega_l$ water is removed from the left TCE and added to the right TCE. If T_l is the water temperature in the left TCE, then an adjustment will be made to extract $\Delta\zeta_l\Omega_l T_l$ from the left TCE and add it to the right TCE in the flux calculation of the temperature equation. The same approach is used for salinity and other scalar variables.

3. Idealized test problems

3.1. Simple seawall overtopping

Consider an overtopping problem in a rectangular channel with a length of 5 km ($2L$) and a width of 1 km (D). A 10-m high (H) vertical seawall is placed at the shoreline at the mid-point ($x = 0$) (Fig. 5a). The ocean side ($x > 0$) features a flat bottom channel filled fully with water, while the land side ($x < 0$) is characterized by a linear slope that is initially dry. The maximum height of the shore is 10 m, the same height as the seawall. The origin of the vertical coordinate ($z = 0$) is defined at the reference water level at the top of the seawall. The model was run with a constant discharge rate Q, which is specified uniformly in the vertical at the open boundary.

Let $t = 0$ at the start of the model run, so that the total volume of inflow from the open boundary at t is Qt. With l being the horizontal distance from the flooding edge to the seawall and h_1 is the water height from the bottom on the land side, then

$$l = \frac{h_1 L}{H} \tag{9}$$

When the land side is completely flooded, we have

$$Qt = \frac{1}{2}lh_1 D = \frac{1}{2}\frac{h_1^2 L}{H}D \tag{10}$$

so that

$$h_1 = \sqrt{\frac{2QH}{LD}t} \tag{11}$$

The overtopping height (h), which is defined as the depth from the reference level, can be determined as

$$h = -\left(H - \sqrt{\frac{2QH}{LD}t}\right) \tag{12}$$

The experiments were made for cases with $Q = 1000 \, \text{m}^3/\text{s}$, $800 \, \text{m}^3/\text{s}$, $600 \, \text{m}^3/\text{s}$, $400 \, \text{m}^3/\text{s}$ and $200 \, \text{m}^3/\text{s}$. For each case, the model was initialized with a 2500-s ramp up and run until $h_1 = H$ (or $h = 0$). The comparison between the model-computed and analytical overtopping heights for all five cases is shown in Fig. 5b. The model accurately matched the analytical solutions. The slight bias near $t = 0$ was due to time-dependent oscillations during the model initial ramp period.

This idealized experiment demonstrates that the dike–groyne algorithm is capable of predicting the volume-conservative overtopping process from the ocean side to the land side.
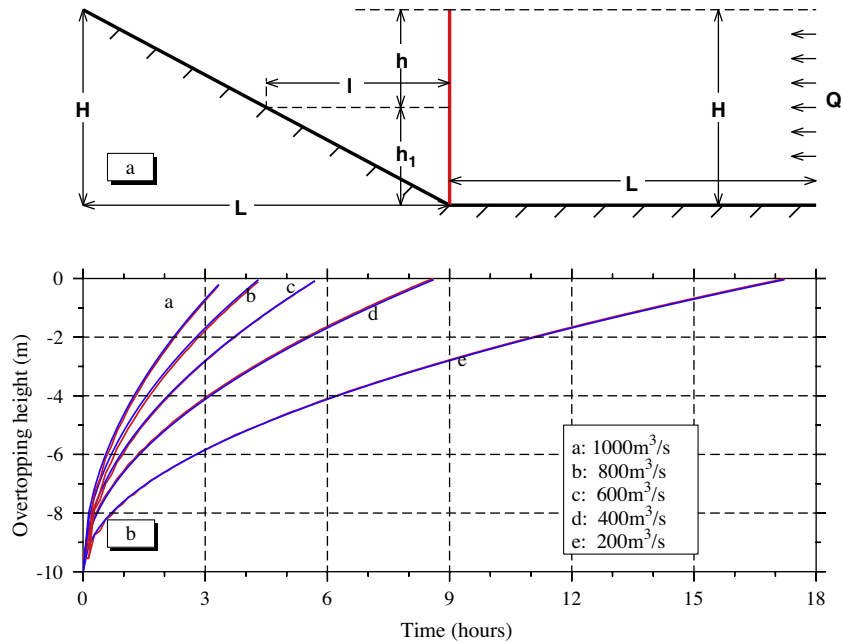
Fig. 5. Schematic of the model set up for the overtopping process experiments (a), model-data comparison of the overtopping depth (b) In panel *a*: *H*: the height of the seawall; *L*: the horizontal length of the land slope and ocean region; *Q*: the water discharge rate at the open boundary, *h*: the overtopping depth from the reference level; h_1: the overtopping height from the bottom; and *l*: the distance from the seawall to the flooded edge on the landside. In panel *b*: blue lines are the analytical solutions, and red lines the model results. (For interpretation of the references to color in this figure legend, the reader is referred to the web version of this article.)

3.2. Eddy formation in a fixed-bed flume with groynes

Yossef and Vriend (2011) (Y&V) conducted a series of laboratory experiments to examine flow features in a fixed-bed flume (schematized as a straight river) with five groynes (Fig. 6). The experiments were made for cases with emerged and submerged groynes. The results suggested that for a given inflow transport, groynes can produce a periodic flow fluctuation and the formation of multiple small-scale eddies between groynes.

We simulate here the Y&V laboratory experiments using FVCOM with inclusion of the dike–groyne module. The numerical experiments were made with the same configuration as the laboratory experiments. The fixed-bed flume is constructed with *x*, *y* and *z* dimensions of 30 m in length, 5 m in width, and 25 cm in height (Fig. 6). Five 2-m long groynes are attached on one side of the flume with a separation distance of 4.5 m. Groynes have a slope edge with a scale shown in the right side panel of Fig. 6. The region off the groynes is defined as the main channel, which is 3 m in width. A constant and uniform water transport is specified as inflow on the left side boundary and the same amount of water transport is specified as

outflow on the right side boundary. Y&V conducted three laboratory experiments: Expt#1 for an emerged condition with water transport $Q = 0.248$ m³/s and flow depth $H = 0.248$ m; Exp#2 for submerged conditions with $Q = 0.305$ m³/s, $H = 0.310$ m; and Exp#3 for submerged conditions with $Q = 0.381$ m³/s, $H = 0.357$ m. Here we consider Exp#1 and Exp#2 for our model validation.

FVCOM was configured with a non-overlapped triangular mesh with a uniform horizontal resolution of 5 cm. A total of ten layers were specified in the vertical, with a vertical resolution of 2.4 cm in the main channel. The vertical and horizontal viscosities were set to have the same Reynolds number of 6×10^4 in the main channel and 10^4 in the groyne region as estimated in the laboratory experiments. The model was integrated for 1000 s, starting with a 100-s ramp up to full flow.

The FVCOM solutions reproduced the flow features observed in the Y&V laboratory experiments. In the emerged groyne case (Exp#1), the laboratory experiment produced three types of eddies between groynes (see Fig. 7 in Y&V): (1) a cyclonic primary eddy in the downstream area between groynes, (2) an anti-cyclonic secondary eddy in the upper-left corner near the left side groyne,
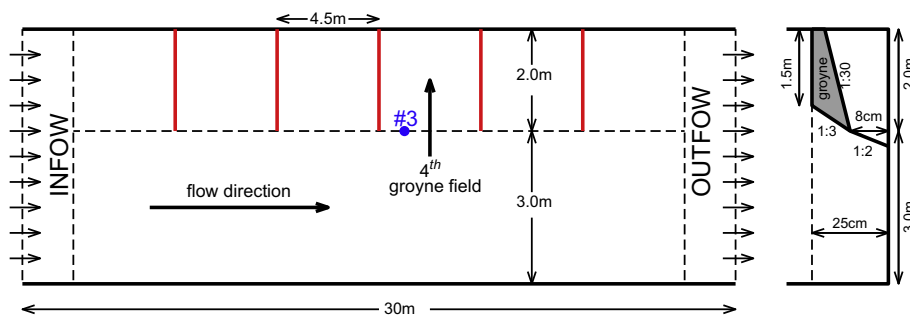
Fig. 6. Plan view of the geometric structure and forcing setup used in the laboratory experiments by Yossef and Vriend (2011) and also used in our numerical experiments. The right panel indicates the cross-sectional view. The gray region is the groyne, and the blue point #3 is the measurement site, which is a distance of 0.75 m from the third groyne tip. The data collecting depth is at 0.3*h* of the whole water column. (For interpretation of the references to color in this figure legend, the reader is referred to the web version of this article.)

and (3) a cyclonic dynamic eddy at the slope edge of the left groyne. These three eddy features were captured in the FVCOM experiment (Fig. 7). The model results not only predict eddy structures, but also the spatial distribution of water exchange between groynes. In the submerged groyne case (Exp#2), a time series of velocity recorded at point#3 (Fig. 6) in the laboratory experiment shows an oscillation with a period of ∼30–35 s. The magnitudes and oscillation periods were captured in the FVCOM experiments (Fig. 8). The high-frequency fluctuations recorded in the laboratory experiment were believed due to sensor noise.

The good agreement seen between these numerical model and laboratory experiments for the emerged and submerged groyne cases demonstrates that the unstructured-grid dike–groyne algorithm implemented in FVCOM correctly captures the dynamics governing flow in such systems.

3.3. Estuary with dikes and groynes

We next applied FVCOM with the dike–groyne module to the estuarine configuration shown in Fig. 9a. This estuary features a spatially uniform bottom depth of 10.0 m with two sets of dikes and groynes placed in the outer region of the estuary. The lengths of the dike and groyne are 7 km and 1 km, respectively, and all dikes and groynes have the same height h above the bottom. The computational domain is discretized using the non-overlapped triangular mesh, with a horizontal resolution varying from 0.1 km around dikes and groynes to 1 km along the lateral boundary and near the open boundary (Fig. 9a).

Two experiments were made with an aim at comparing two methodologies: one in which the dikes and groynes are treated as a bed-conforming slope (Fig. 10a) and the other in which the dike and groynes are constructed using the algorithms described in (2)–(8) (Fig. 10b). In the vertical direction, a sigma coordinate with uniform layer thickness was used for both cases (Fig. 10). The sigma coordinate is a terrain-following coordinate, with levels parallel to the bed-conforming slope in the first and to the flat bottom in the second case. In both cases, the model was driven only by the M_2 (period: 12.42 h) tidal elevation with amplitude 1.0 m at the open boundary. The model was spun up from zero velocity

and surface elevation with a constant salinity of 35 psu specified at all nodes at initialization.

The experiments were conducted using multi-processor computers with the MPI-based domain decomposition (Fig. 9b). To improve the parallelized computational efficiency, the neighboring nodes and cells connected to dikes and groynes were defined as an independent sub-domain (red and blue colored regions) and run separately using a master node.

We ran the model with different values of h. The model results show that in both cases, the influence of dikes and groynes on the currents and sea level varies with h, vanishing at $h = 0$ and increasing as h is increased. For given h, however, the flow fields predicted in these two cases differ significantly. An example for $h = 5$ m (one half the mean water depth) is shown in Fig. 11. In the dike–groyne algorithm case, the deeper flow is blocked by the submerged construction, causing an anti-cyclonic shear flow around the groyne during the flood tidal current (Fig. 11: right panels). In the bed-conforming slope case, the water flows over the groyne, with no clear blocked flow features (Fig. 11: left panels). The difference can be viewed more clearly on the flow distribution on the along-channel section (Fig. 12). With the dike–groyne treatment, no flux onto the wall tends to turn the flow along the wall not only in the blocked region but also in the upper unblocked region, while the bed-conforming slope method predicts that the water flows over the wall along the slope.

This idealized case clearly shows that difference between the bed-conforming slope method and dike–groyne algorithm around the submerged structure. Yossef (2005) and Uijttewaal (2005) found significant eddy fluctuations under submerged groyne conditions, which appeared in the experiment with dike–groyne algorithm but not in the experiment with the bed-conforming slope. The bed-conforming slope method allows the water to flow over the slope as a sloping bottom boundary current, and can significantly underestimate the retention effect due to eddies formed around the construction.

We also conducted the same experiments with temperature stratification. In the bed-conforming slope method, tidal mixing can create a thermal boundary layer over the slope, which can produce shear flows near the bottom (Chen and Beardsley, 1998),
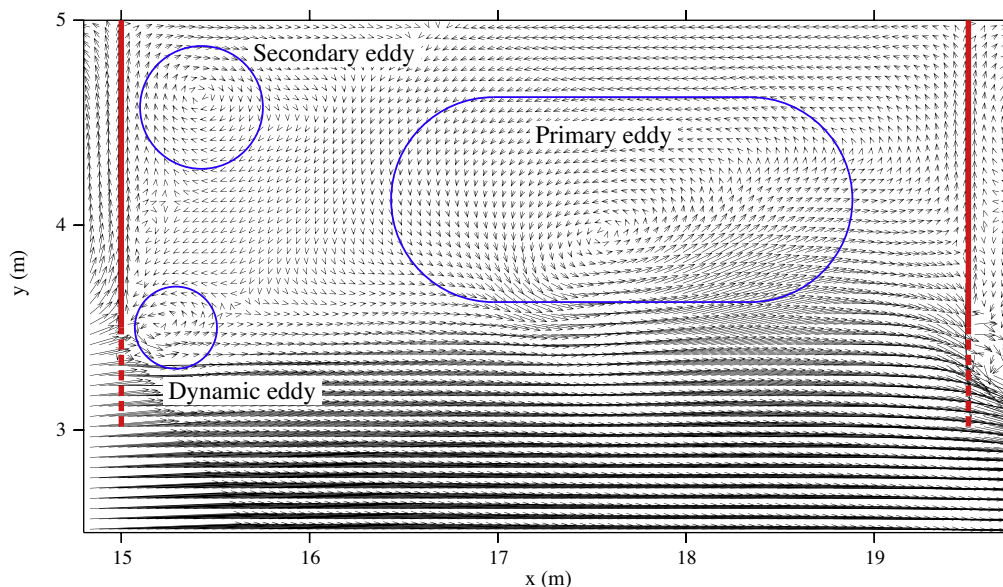
Fig. 7. Snapshot of simulated flow patterns in the fourth groyne field for Exp#1 under an emerged groyne condition. Solid red lines indicate emerged groynes, and dashed red lines indicate the submerged slope edges of groynes. Blue cycles show the locations of primary, secondary and dynamic eddies. (For interpretation of the references to color in this figure legend, the reader is referred to the web version of this article.)
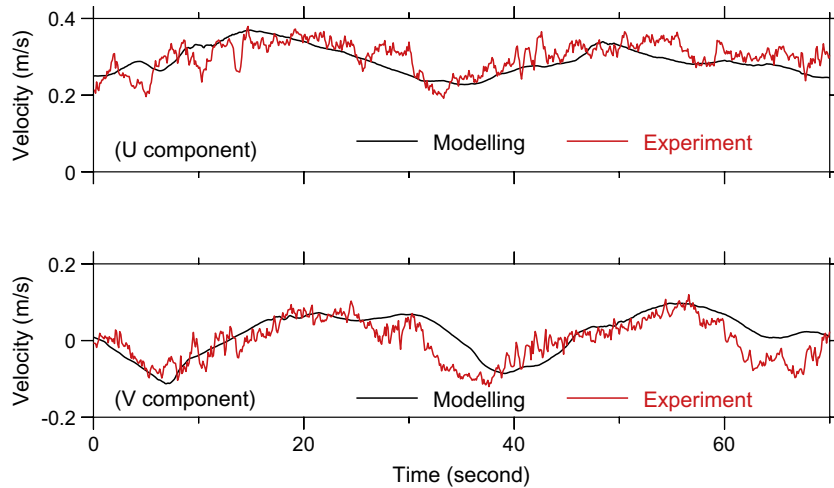
Fig. 8. The model-data comparison of *u* and *v* components of the fluid velocity at point #3 for Exp#1 under a submerged groyne condition. Red lines indicate the time series of the measured velocity recorded in the laboratory experiment and black lines are the model-computed velocity. (For interpretation of the references to color in this figure legend, the reader is referred to the web version of this article.)
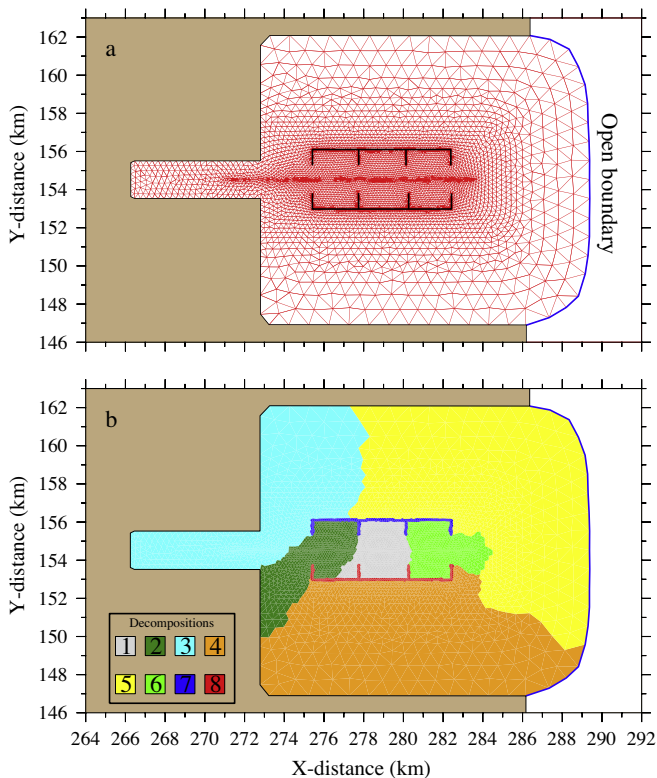
Fig. 9. The computational domain and unstructured triangular mesh (a) and domain decomposition (b) for the idealized estuary case. Bold solid lines inside the domain are the dikes and groynes specified in the model.

Fig. 10. The vertical structures of the terrain-following coordinate levels in the bed-conforming method (a) and dike–groyne treatment method (b).

which differ from the blocked flow features predicted in the dike–groyne treatment.

4. Application to the Changjiang Estuary

The Changjiang is the largest river flowing into the East China Sea (ECS) (Fig. 13), with an annually-averaged freshwater discharge rate of 28,527 m³/s, for a total annual freshwater discharge of $\sim 9 \times 10^{11}$ m³ (Chen et al., 1994, 1999; Hu et al., 2002; Liu,

2008). The river outflow varies significantly with season: $\sim 60,000$ m³/s or greater in the flood season (May through October), and $\sim 10,000$ m³/s in the dry season (November through April). In recent history, the maximum discharge rate was 92,600 m³/s in August 1954 and the minimum rate was 4620 m³/s in January 1979. The Changjiang is also a major source of sediment to the ECS, with a total annual amount of 4.86×10^{8} tons before the 1990s (Chen et al., 1999) and about 2.0×10^{8} tons after the 1990s.

The large amount of sediment deposition in the shipping route has restricted navigation in the Changjiang Estuary. The Deep Waterway Channel Regulation Project (DWCRP) off the Changjiang was launched in 1998 to improve navigation conditions around the estuary (Jin et al., 2003). In phase I of this project, a set of dikes and groynes were constructed along the North Passage (Fig. 13). The dikes were designed near the mean tidal level to block the tidal current and thus sediment transport. Enhancing the current separation at the riverward head of the dikes reduced water flow into the channel during the ebb tide by 88% (Chen and Le, 2005). Between these dikes, a set of groynes were constructed perpendicularly to each dike, with an expectation of increasing the sediment erosion and maintaining the water depth in the main navigation path as a result of the intensity of the currents along the channel (Le et al., 2006). The groyne is connected to the dike with the same elevation and then decreases linearly to a depth of 2.0 m below mean sea level. This phase I project was completed in 2001, with
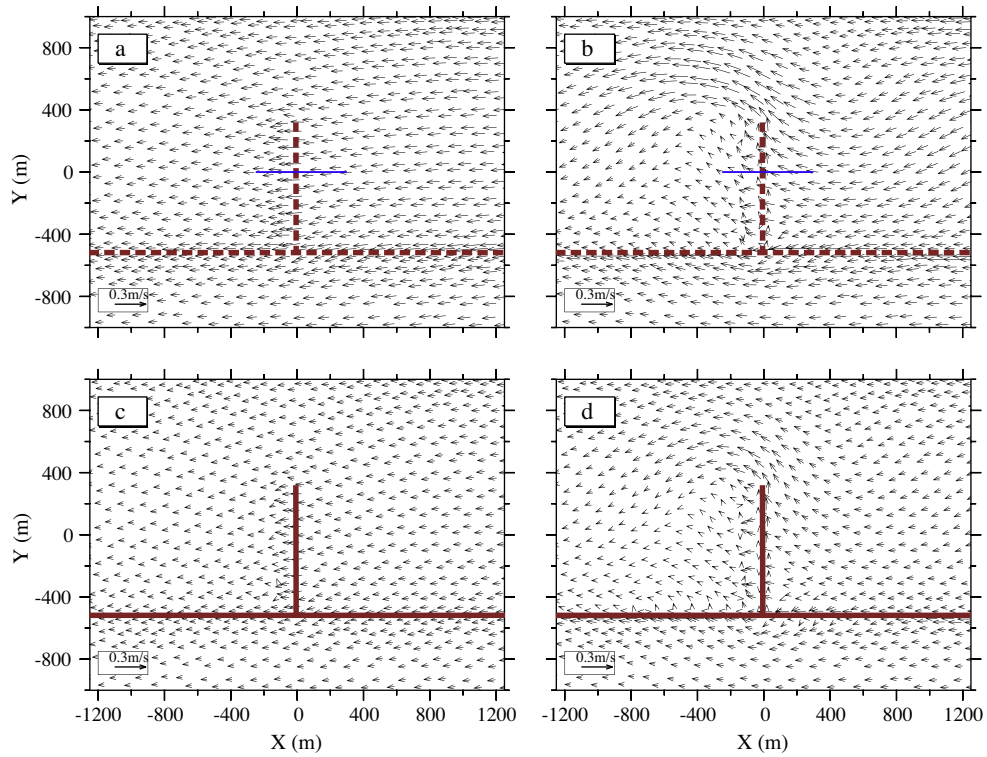
Fig. 11. Distributions of horizontal currents near the surface (upper row) and bottom (lower row) for the idealized estuary case driven by tidal forcing with slope bed-conforming method (left column) and the dike–groyne algorithm (right column). The blue solid lines in the upper row panels indicate the location of the velocity sections shown in Fig. 12. (For interpretation of the references to color in this figure legend, the reader is referred to the web version of this article.)
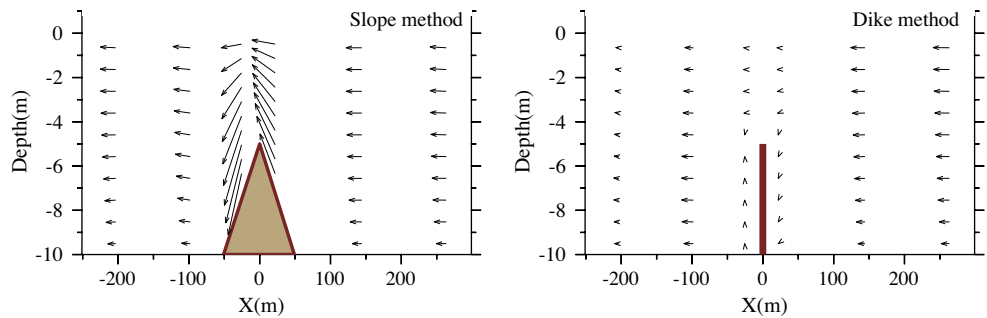
Fig. 12. Velocity distributions along the vertical section under slope-conforming method (left) and dike–groyne algorithm (right). The horizontal position of the vertical section is shown in Fig. 11.

a goal of producing and maintaining a water depth of 8.5 m in the channel in 2002 (Fan, 2004; Fan and Wu, 2004). The phase II project started in 2002 and was completed in June 2005, with the aim of increasing water depth in the channel to 10 m (Fan, 2004; Jin and Huang, 2005; Jin and Zhu, 2005). In this phase, the dikes were extended seaward, the additional groynes (five on the north and four on the south) were added and the lengths of pre-constructed groynes were increased.

Since these dikes extend about 0.3 m above mean sea level and have a width of several meters, they become both exposed and submerged over a tidal cycle. Previous modeling studies (Du, 2007; Qi, 2003; Wu, 2006) treated these structures as submerged "sills" (following the bed-conforming slope method) and failed to reveal two-layer dynamics around the structures. The thin-dam method of DeLft3D-FLOW was also applied to resolve dike–groyne structures in this region (Hu et al., 2009). This model, however,

experienced difficulties in resolving the realistic and irregular geometries of the dikes and groyne. We have selected this region as a testbed problem to compare the bed-conforming slope method used in previous studies (Du, 2007; Qi, 2003; Wu, 2006) and the dike–groyne algorithm developed in this paper. Both simulations were conducted within the FVCOM framework, but with the bed-conforming slope method and dike–groyne algorithm implemented respectively to treat the dike–groyne structures in the river mouth.

The numerical experiments were conducted using FVCOM through a nesting of regional and local computational domains. The regional domain covers the entire ECS with the full physical setup described in Chen et al. (2008), while the local domain includes the Changjiang Estuary from the upstream source to the offshore region at about 124.5°E and from 28.3°N to 34.3°N (Fig. 14). Both domains were configured using a non-overlapping triangular
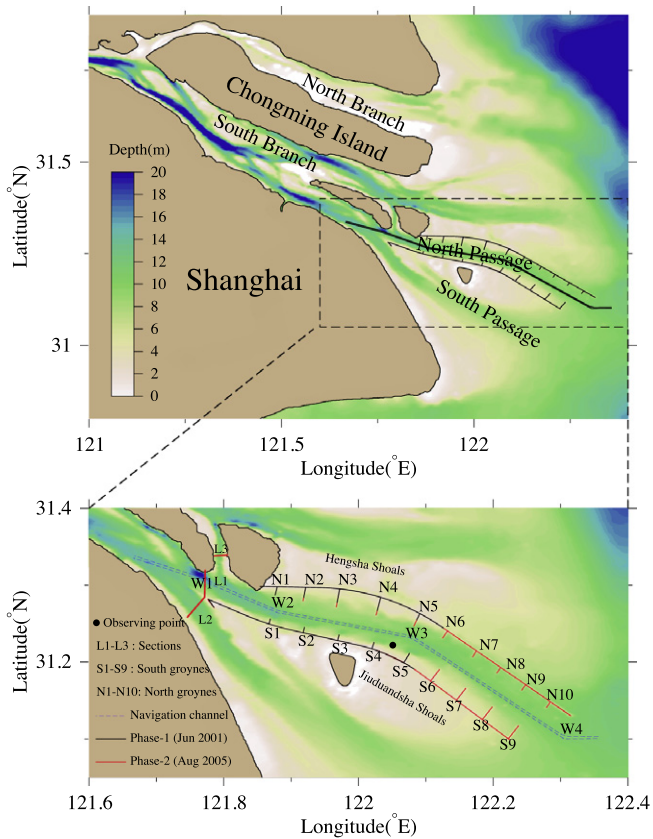
Fig. 13. Upper panel: bathymetry of the Changjiang Estuary and adjacent inner shelf region of the East China Sea. Black lines around the North Passage represent the dike and groyne construction built during the Deep Waterway Channel Regulation Project. The bold black line in the middle of the North Passage is the navigational channel. Lower panel: a detailed Phase I and Phase II project layout. The black solid lines denote the dikes and groynes built during the Phase I project; the red lines denote the construction modified and added during the Phase II project. The dashed blue lines mark the navigational route. N1-N10 and S1-S9 represent the ten northern and nine southern groynes, respectively. The magenta lines L1, L2 and L3, are the sections selected to calculate the ratio of the water transport entering the Deepway Channel to the total transport flowing out from the southern branch of the Changjiang. (For interpretation of the references to color in this figure legend, the reader is referred to the web version of this article.)

mesh in the horizontal and generalized terrain-following coordinate transformation in the vertical. The ECS mesh features about
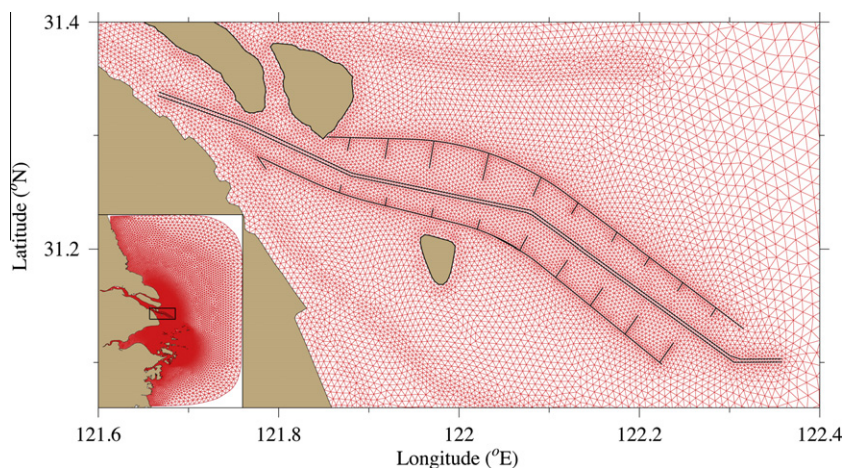
240,000 cells with a horizontal resolution of 1.0–15 km, while the local Changjiang Estuary mesh features about 100,000 cells with the finest resolution of about 200 m located around the Deep Waterway structures (see right panel in Fig. 14 for an enlarged view). The time step was 2 min for the regional ECS domain and 10 s for the local Changjiang Estuary domain. This nesting approach improved the overall computational efficiency by a factor of 10.

The dikes and groynes were placed in the Deep Waterway area as zero-width solid walls (solid dark lines) in the local computational domain. The geometric shapes of these constructions are represented accurately using the triangular meshes. Given an average tidal range of about 2.6 m around the Changjiang Estuary, the dikes and groynes should be about 1.5–2.0 m below water during high tide.

The local domain FVCOM is driven by eight major astronomical tidal constituents—M_2, S_2, K_2, N_2, K_1, O_1, P_1 and Q_1—through nesting with the regional ECS FVCOM (Chen et al., 2008) at the outer open boundary and freshwater discharge at the upstream end of the Changjiang and at the location of the Qiantang River in Hangzhou Bay (Ge et al., 2008). Experiments were conducted for the typical flood (40,000 m³/s) season and typical dry (10,000 m³/s) season freshwater discharge conditions. In both cases, the discharge rate for the Qiantang River is specified as 1000 m³/s. To examine the change in hydrodynamic conditions after the Phase II project construction, we ran the model with dikes and groynes constructed using both the bed-conforming slope method and the dike–groyne algorithm, respectively.

The turbulence mixing in these experiments was parameterized using the same method used in Chen et al. (2008) and Xue et al. (2009). The horizontal diffusion coefficient was calculated using the Smagorinsky (1963) turbulent closure scheme and the vertical eddy viscosity and thermal/salt diffusivity were determined using the Mellor-Yamada 2.5-level turbulence closure model (Mellor and Yamada, 1982).

4.1. Current structure

The current structure changed significantly after the dike–groyne construction was completed. With the M_2 being the dominant tidal component, Jiuduansha Shoal with the south dike built along its northern edge separates the water flow into two branches as shown in Fig. 15a–b. We define the ratio of water transport into the navigation channel to the total outflow from the southern branch of the Changjiang as

Fig. 14. Enlarged view of the triangular mesh with dikes and groynes around the Deepway Channel off the Changjiang. The panel inserted in the lower left corner shows the computational domain and mesh of the local domain FVCOM with inclusion of the Changjiang, Hangzhou Bay and the inner shelf of the East China Sea.

$$R = \frac{F_N}{F_N + F_s} \times 100\% \qquad (13)$$

where F_N and F_s are the volume fluxes flowing through sections L1 and L2 (shown in Fig. 13), respectively. Field measurements indicate that R dropped from 60% in August 1998 to 40% in August 2006 (Liu, 2008). Before the Phase I project, the North Passage was the main channel for the Changjiang outflow. During that period, R was above 50%. Since 2000, R dropped to 50%, and now is about 40%. After the Phase I project, the model-computed R was 48 ± 1.0%, agreeing well with the observed value of 49% reported in August 2000 (Table 1).

After the Phase II project, the model-computed ratio dropped to 42 ± 1.0%, which is close to the observed value of 45% reported in August 2005. This suggests that extending the dikes seaward, elongating existing groynes, and adding more groynes in the extended region do have a significant impact on the current separation at the upstream tip of the southern dike.

The model shows that the construction of groynes along the dikes produces residual cyclonic eddies and anti-cyclonic eddies between groynes in the northern and southern regions, respectively (Fig. 15). Eddy size depends on groyne length. Elongating the groynes in the Phase II project tends to intensify eddies
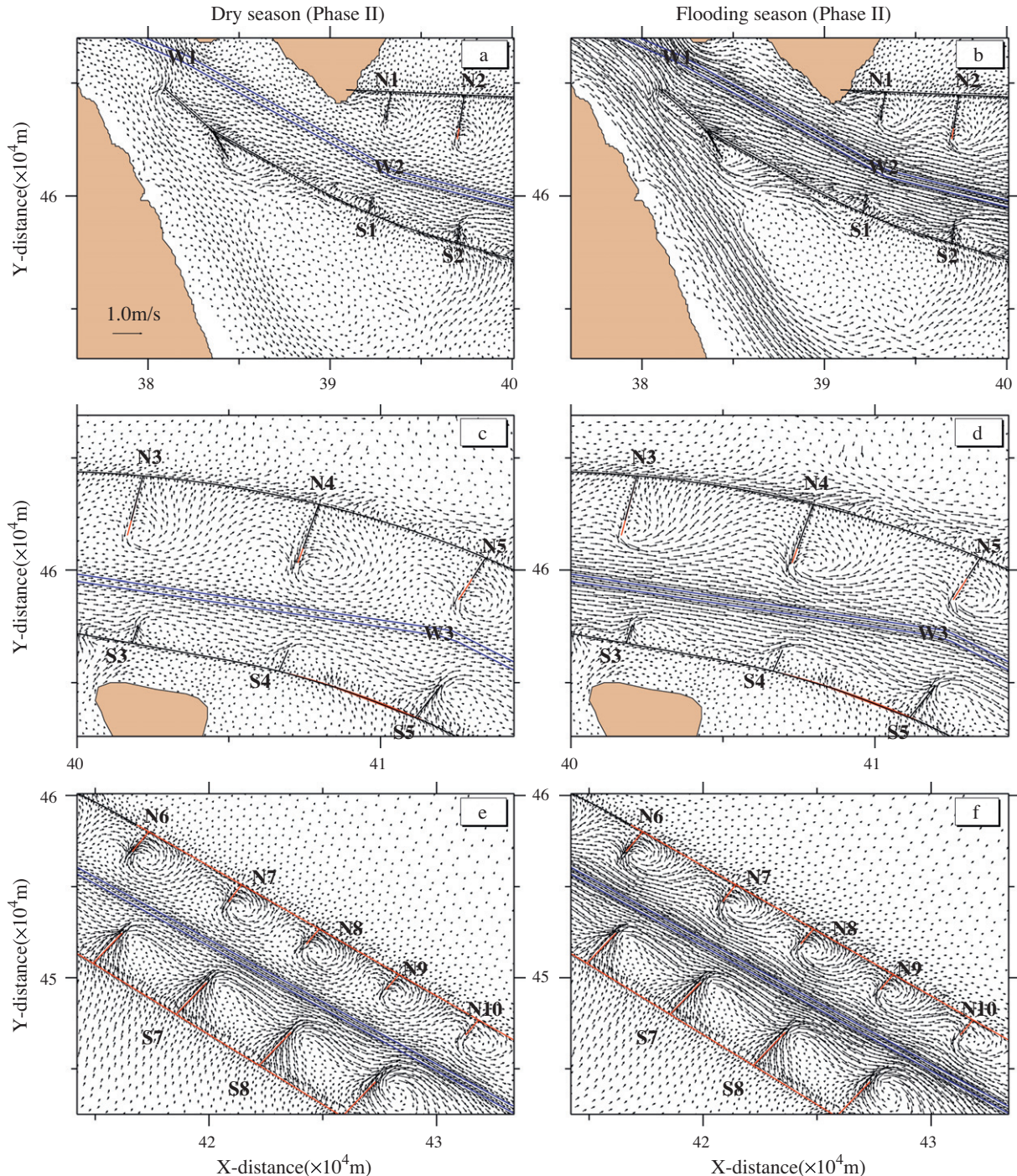
Fig. 15. Distributions of residual currents around the Deep Channel predicted by FVCOM under the freshwater discharge condition for the dry season (left column) and flood season (right column) with dike–groyne algorithm.

Table 1
Comparison of the observed and model-predicted ratios of the water flux through section L1 to the sum of the water flux through sections L1 and L2 after Phase I and Phase II projects. The ratio is defined as Eq. (13) in the text.

	Phase-I		Phase-II	
	Flood (%)	Dry (%)	Flood (%)	Dry (%)
Observed ratio	49	/	45	/
Modeled ratio	48 ± 1	47 ± 2	42 ± 1	41.3 ± 2

between N3 and N5. Extending dikes seaward and adding more groynes not only seems to significantly speed up water flow in the central water passage in the downstream area, but also causes a net cross-dike inflow into the navigation path around the north-western side of Jiuduansha Shoal (between S5 and S9) and more eddies in the downstream area (Fig. 15).

The current pattern remains unchanged during spring and neap tides, although eddies and cross-dike flow intensify during spring tide and weaken during neap tide (Fig. 16). When the Phase I project was completed, the difference in maximum velocity along the navigation channel between spring and neap tides was about 0.28 m/s during the ebb period and about 0.72 m/s during the flood period (Table 2). The angle of the tidal currents to the axis of the navigation channel was in the range of 6.4–6.7° at the maximum ebb and 7.0–8.9° at the maximum flood. The Phase II project resulted in a minor change in the velocity but a significant reduction in the angle of tidal currents to the axis of the navigation channel by at least 50%. This indicates that extending dikes seaward tends to concentrate the water along the channel, but has little impact on the water flux through the channel.

Although the freshwater discharge rates strongly differ between the flood season (40,000 m³/s or up) and dry season (~10,000 m³/s), the cross-dike residual current seems relatively unchanged since it is mainly caused by the astronomical tide which is not affected by the upstream Changjiang runoff. The cross-dike current occurring along the south and north dikes in a south-to-north direction implies that significant net water transport exists from the Jiuduansha Shoal into the North Passage along the south dike, and from the North Passage to Hengsha Shoal along the north dike (Fig. 16).

The model experiment results show that the Deep Waterway Channel Regulation Project has achieved its major goal of increasing and maintaining the depth in the navigation channel up to 8.5 m after Phase I in 2002, and 10.0 m after Phase II in June 2005. However, the persistence of eddies between groynes and the bathymetric change due to morphology can cause a dramatic amount of sediment accumulation inside the dike–groyne complex. This prediction is consistent with recent sediment measurements in that region, suggesting that dikes and groynes built along the navigation channel will not be able to meet the expected objective of the original design to block all south-to-north sediment transport from Jiuduansha Shoal.
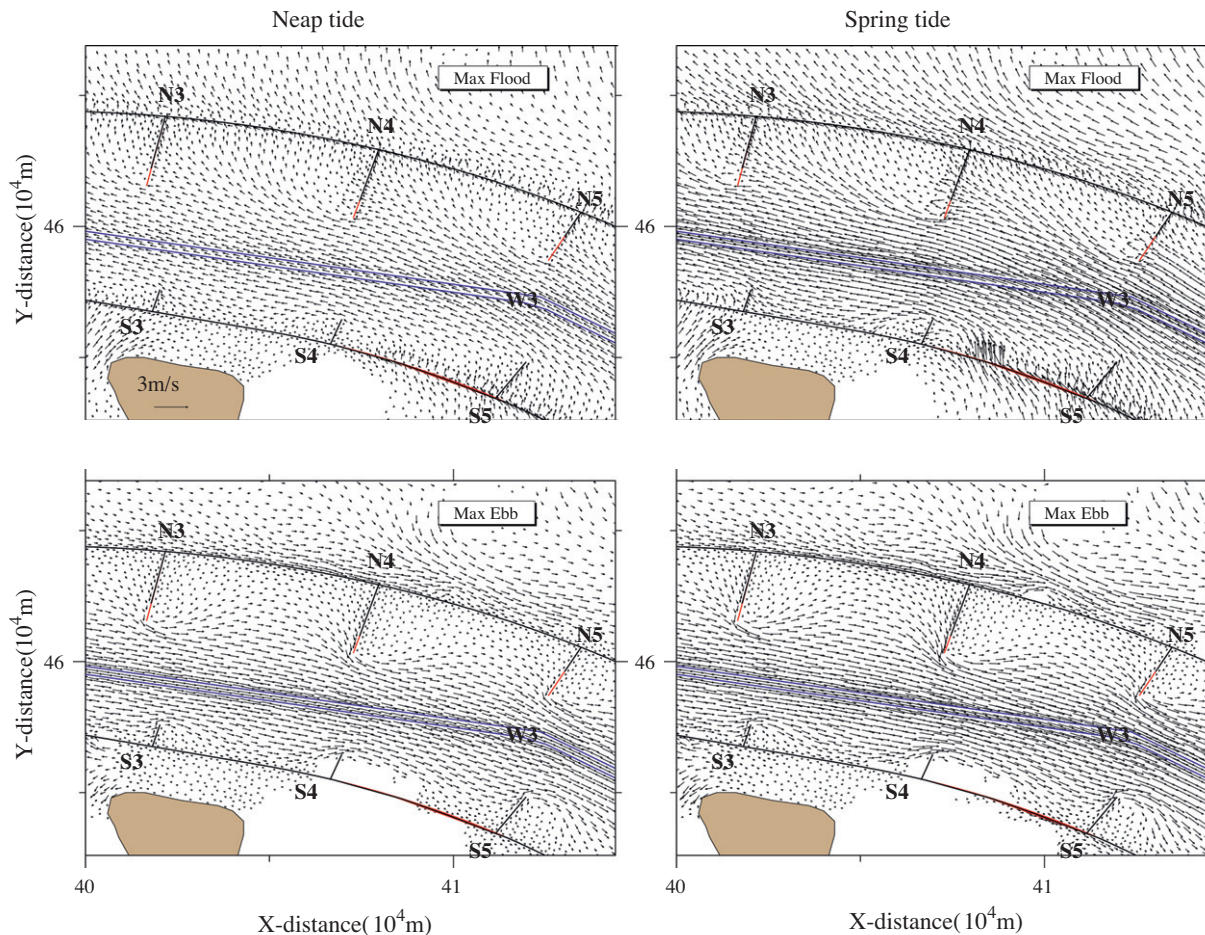
Fig. 16. Distributions of currents near the surface at maximum flood (upper row) and ebb (lower row) between the segments marked W2–W3 during the spring tide cycle (right column) and neap tide cycle (left column) in the flooding season predicted by FVCOM with dike–groyne algorithm.

Table 2
Angle and speed of the currents with respect to the axis of the navigational route under spring and neap tidal conditions for flood and dry seasons, respectively.

	Phase I				Phase II			
	Max. ebb		Max. flood		Max. ebb		Max. flood	
	θ (°)	V (m/s)	θ (°)	V (m/s)	θ (°)	V (m/s)	θ (°)	V (m/s)
Flood season (neap)	6.4	1.25	8.9	0.71	3.0	1.29	2.9	0.73
Flood season (spring)	6.7	1.53	7.0	1.43	3.1	1.53	3.5	1.45
Dry season (neap)	6.8	1.16	8.4	0.97	3.3	1.11	3.2	1.01
Dry season (spring)	6.6	1.28	6.3	1.73	2.7	1.38	2.1	1.79

4.2. Comparison between dike–groyne and bed-comforting slope methods

The model results obtained using the dike–groyne algorithm and the bed-conforming slope methods are compared here with observational data. The field measurements were made inside the navigation channel near W3 (the site marked by the black solid circle in Fig. 13) during the flood periods in February 2006. The model-data comparisons were made for current speed and direction at near-surface, mid-depth and near-bottom levels (Fig. 17). Both methods were robust in simulating the water currents and transport around the DWCRP in this realistic situation (Fig. 17). However, the average standard deviation between modeled and observed velocities, estimated over the measurement period, was 17 cm/s for the dike–groyne algorithm case and 23 cm/s for the bed-conforming slope case. The major improvement of the dike algorithm appeared during high tide, when the average standard deviation was ∼4 cm/s for the dike–groyne case and ∼15 cm/s for the bed-conforming case. As a result, the model-predicted phase of the flow peak and trough showed a better match with observations in the dike–groyne algorithm case than in the bed-

conforming slope case. The bed-conforming slope method leads to an overestimation and underestimation of the current peak at the surface (and mid-depth) in comparison to near-bottom, respectively, suggesting that it produces a stronger vertical velocity shear than the dike–groyne algorithm.

For the given initial conditions and forcing, the salinity predicted at W3 by these two methods significantly differed. The measurements were made in the dry season during which the river discharge was of order 10,000 m³/s. The site W3 was located within the transition zone between the Changjiang discharge dilute and ocean salt waters, with a minimum salinity as low as ∼2 psu. The dike–groyne algorithm-predicted time series of salinity shows a better match with the data at the surface, mid-depth and near the bottom (Fig. 18), while the bed-conforming slope method overestimated the salinity by a value of 8 psu or more.

The difference can be also viewed in the horizontal distributions of salinity at the surface and near the bottom. An example is shown in Fig. 19 for a comparison for surface and bottom salinity at maximum ebb tide in the flood season. In the bed-conforming slope case, the high-salinity water from the surface to bottom dominates the navigation channel region and the salinity around the dikes
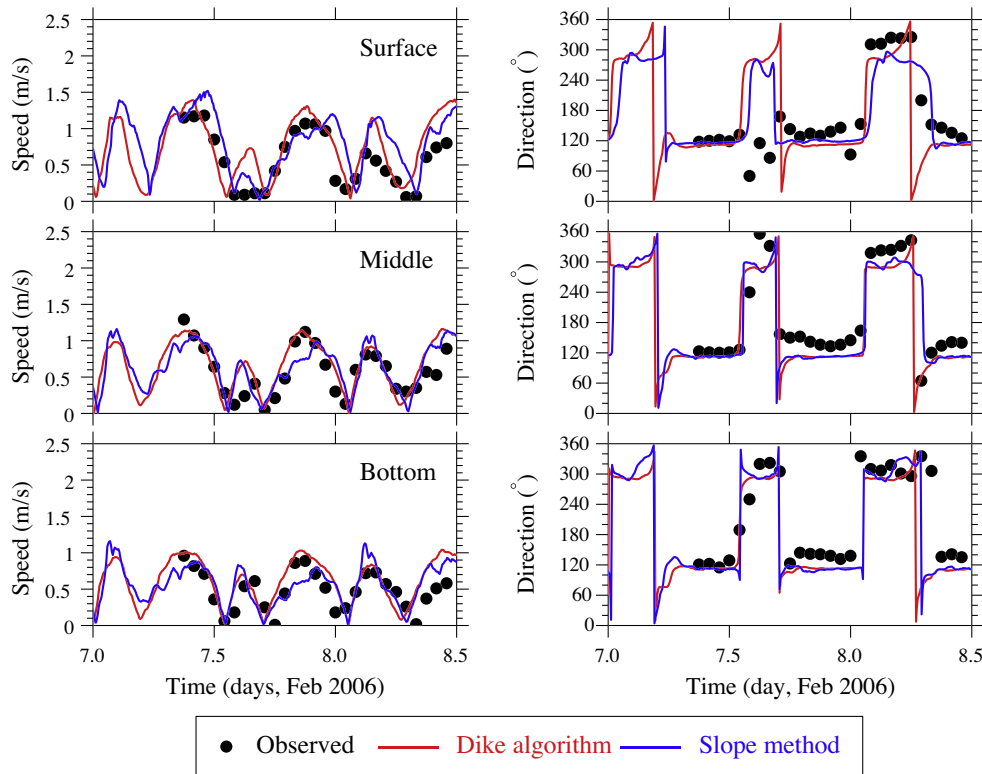
Fig. 17. Model-data comparisons of current velocity (left) and direction (right) during February 2006 at the surface (upper), mid-depth (middle) and near bottom (lower). The solid black dots indicate the field data. The blue and red lines indicate the results with the dike–groyne algorithm and bed-conforming slope method, respectively. (For interpretation of the references to color in this figure legend, the reader is referred to the web version of this article.)

Fig. 18. Model-data comparisons of the salinity in February 2006 at the surface, mid-depth and near bottom. The solid black dots indicate the field data. The blue and red lines indicate the results with the dike–groyne algorithm and bed-conforming slope method, respectively. (For interpretation of the references to color in this figure legend, the reader is referred to the web version of this article.)
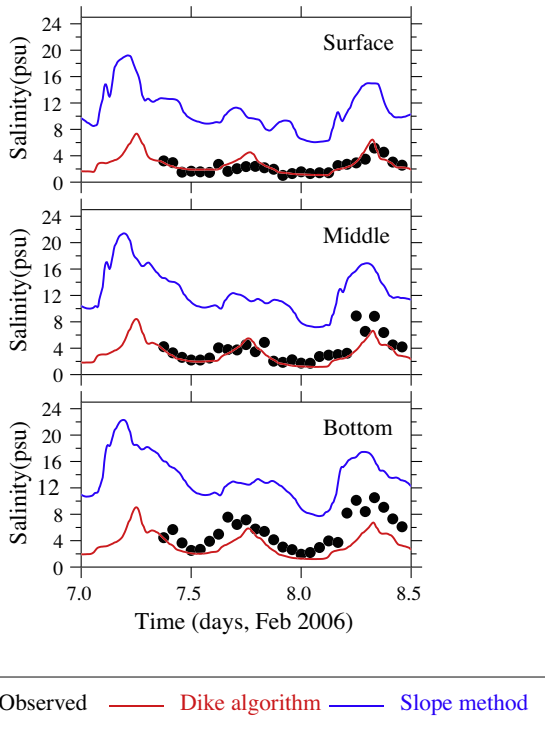
and groynes is relatively spatially uniform. In the dike–groyne algorithm case, the model predicts a large vertical gradient in the navigation channel. At the surface, the water is dominated by the low-salinity mixed Changjiang discharge flow, while relatively high salinity water remains near the bottom in the navigation channel during the offshore flow period. During the ebb tide, the dikes become exposed above the sea surface, and act more as a solid barrier for the water exchange between the channel and surrounding area. That can be seen in the area between N6 and N10. Similar features also appear in the region between groynes S6 to S9.

5. Discussion and conclusions

An unstructured-grid finite-volume dike–groyne treatment algorithm is derived and implemented into FVCOM as a module. The unstructured triangular mesh used in this model is flexible to accurately resolve any configuration of dikes and groynes, and the finite-volume flux algorithm in FVCOM ensures the conservation of volume and mass under the boundary condition of no flux into or out of the structure. With the same MPI framework, this model can be run efficiently on a single computer or multi-processor cluster for fast computation.

The idealized test cases are designed to validate the capability of the dike–groyne module in resolving realistic water exchange around and over a dike–groyne structure and overtopping of a seawall onto dry land plus accuracy of parallel computing under memory-distributed multiple-node architecture. The comparisons between the dike–groyne algorithm and the bed-conforming slope method suggests that resolving the kinematic boundary condition on dike–groyne structures is critical to capturing realistic flow and tracer fields in the system. The bed-conforming slope approach can
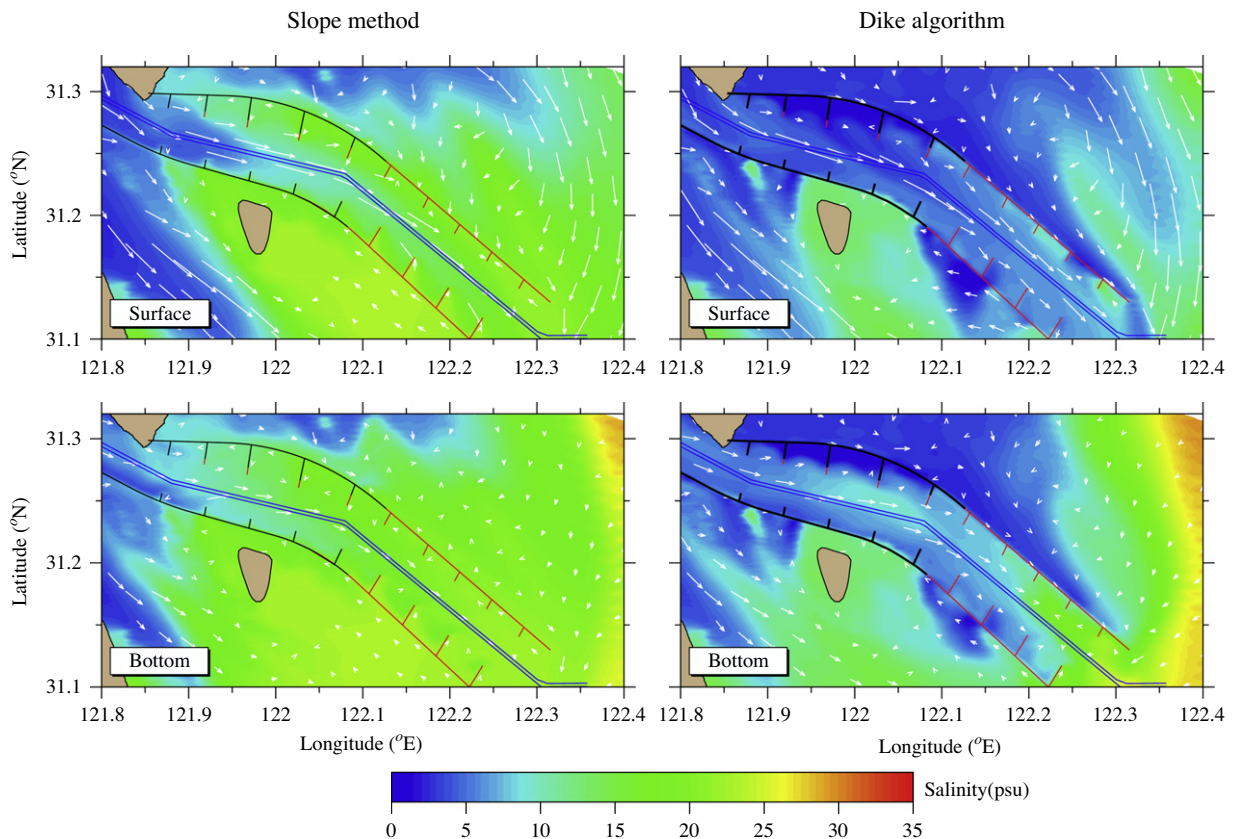
Fig. 19. Model-predicted distributions of the salinity near the surface (upper) and bottom (lower) at maximum ebb tide around the Deep Waterway Channel Regulation Project during spring tide of the flooding season for the cases with bed-conforming slope method (left) and dike–groyne algorithm (right).

cause an unrealistic overestimation of water transport across the structure and poor resolution of the geometrically controlled eddies formed around the structure. The overtopping experiment demonstrates that the dike–groyne algorithm is capable of predicting the volume-conservative overtopping process from the ocean side to the dry land side.

The dike–groyne module is used to simulate the flow field in the Changjiang Estuary where a series of dikes and groynes have been recently built as part of the Deep Waterway Channel Regulation Project. The model results indicate that the construction of the dike–groyne system does reduce the proportion of the Changjiang's southern branch outflow water entering the navigation channel. The comparison for the cases with the dike–groyne algorithm and bed-conforming slope method suggests that due to the change of the horizontal and vertical distribution of currents, the bed-comforting slope method predicts significantly different features of vertical mixing and water exchange between the Changjiang dilute water and higher-salinity ocean waters in the navigation channel. The better model-data comparison results obtained with the dike–groyne algorithm supports the need to implement this method to improve model simulations of the complex currents and turbulent mixing in dike–groyne systems in coastal and estuarine regions.

It should be pointed out here that the overtopping algorithm in the FVCOM dike–groyne module was derived using volume conservation to estimate how much water can flood from one side to another side without consideration of the overtopping dynamics. The overtopping process can be very complex, including for example hydraulic drop-induced head loss and wave- and wind-driven "splash-over", and varies widely in different sites as a function of different geometries, forcing conditions and dynamics. A number of investigators (e.g. McCoy et al., 2006, 2008) have begun to use Large Eddy Simulation approaches with non-hydrostatic dynamics and air–water interaction to explore the different dynamical processes involved in overtopping while others (e.g. Kees et al., 2011) have developed level set and volume-of-fluid approaches to two-fluid incompressible flow and are applying these new methods to study transient wave- and wind-driven flow over coastal barriers. We plan to follow this new work closely and examine if their new results can be used to extend the FVCOM dike–groyne module to simulate more directly overtopping in realistic settings.

Acknowledgements

Appendix A

The dike–groyne module was coded into FVCOM within the MPI parallel environment. We have tested the computational efficiency using the dike–groyne module, which depends on the numbers of dikes and groynes configured in the grid. A key factor that can affect the parallelization efficiency is the data exchange among processors. The code in FVCOM version 3.1 and higher allows model data-exchange between individual processors. Since dikes and groynes may cross multi-domains, including dikes and groynes in the MPI domain could decrease the computational efficiency. To solve this problem, we used a dynamical domain decomposition method, in which we temporally store all triangle nodes and cells connecting to dikes and groynes into an independent processor and compute separately. With this approach, the imbalance of the computation load in the parallel environment is greatly improved. For the idealized estuarine experiment described in Section 3.3, using 4 Intel® Core® i7 2.2 GHz processors, the model simulation took 93 min in the bed-conforming slope case and 116 min in the dike–groyne algorithm case. For the Changjiang Estuary case described in Section 4, using 8 Intel® Xeon® E5335 2.00 GHz processors (totally 32 parallel threads) on the East China Normal University Linux cluster, a one-month model simulation took 24.5 h in the bed-conforming slope case and 31.0 h in the dike–groyne algorithm case. In our cases, using the dike–groyne algorithm increased the computational time by ~25%.

References

Allsop, W., Bruce, T., Pullen, T., van der Meer, J., 2009. Hazards from wave overtopping, Flood Risk Management – Research and Practice, Proceedings of FLOODrisk, Keble College, Oxford, UK.

Chen, C., Beardsley, R., Limeburner, R., 1994. Comparison of winter and summer hydrographic observations in the Yellow and East China Seas and adjacent Kuroshio during 1986. Continental Shelf Research 14, 909–929.

Chen, J.Y., Li, D.J., Chen, B., Hu, F., Zhu, H., Liu, C., 1999. The processes of dynamic sedimentation in the Changjiang Estuary. Journal of Sea Research 41 (1–2), 129–140. doi:10.1016/S1385-1101 (98) 00047-1.

Chen, C., Liu, H., Beardsley, R.C., 2003. An unstructured, finite-volume, three-dimensional, primitive equation ocean model: application to coastal ocean and estuaries. Journal of Atmospheric and Oceanic Technology 20, 159–186.

Chen, C., Beardsley, R.C., 1998. Tidal mixing over finite-amplitude banks: a model study with application to Georges Bank. Journal of Marine Research 56 (6), 1163–1203.

Chen, Z., Le, J., 2005. Regulation principle of the Yangtze River Estuary deep channel. Hydro-science and engineering 1, 1–8 (in Chinese).

Chen, C., Cowles, G., Beardsley, R.C., 2006a. An unstructured grid, finite-volume coastal ocean model: FVCOM User Manual, Second Edition, SMAST/UMASSD Technical Report-06-0602, p. 45.

Chen, C., Beardsley, R.C., Cowles, G., 2006b. An unstructured grid, finite-volume coastal ocean model (FVCOM) system, Special Issue entitled "Advance in Computational Oceanography". Oceanography 19 (1), 78–89.

Chen, C., Huang, H., Beardsley, R.C., Liu, H., Xu, Q., Cowles, G., 2007. A finite-volume numerical approach for coastal ocean circulation studies: comparisons with finite difference models. Journal of Geophysical Research 112. doi:10.1029/2006JC003485, C03018.

Chen, C., Xue, P., Ding, P., Beardsley, R.C., Xu, Q., Gao, G., Qi, J., Li, C., Lin, H., Cowles, G., Shi, M., 2008. Physical mechanisms for the offshore detachment of the Changjiang diluted water in the East China Sea. Journal of Geophysical Research 113. doi:10.1029/2006JC003994, C02002.

Cowles, G., 2008. Parallelization of the FVCOM coastal ocean model. International Journal of High Performance Computing 22 (2), 177–193.

Delft3D-FLOW User Manual, 2009. Simulation of multi-dimensional hydrodynamic flows and transport phenomena, including sediments, Deltares, Rotterdamseweg 185, P. O. Box 177, 2600 MH Delft, The Netherlands.

Du, P., 2007. Sediment Transport Research in Yangtze Estuary and Hangzhou Bay, Doctoral dissertation of East China Normal University, pp134 (in Chinese).

Fan, Q., 2004. The Innovation of the Yangtze Estuary Deepwater Channel Improvement Project. Engineering Science in China 6 (12), 13–28 (in Chinese).

Fan, Q., Wu, P., 2004. Review for the integrated engineering techniques applied in the constructions of the major shipping channels and ports in 2004. China Civil Engineering Journal 38 (9), 20–25 (in Chinese).

Ge, J., Ding, P., Chen, C., Xue, P., 2008. Low-salinity plume in the Changjiang and adjacent coastal regions: a model-data comparison, Proceedings of the 31st International Conference of Coastal Engineering 2008. Hamburg, Germany, pp. 4471–4481.

Hu, F., Hu, H., Gu, G., 2002. Studies of fronts in the Changjiang Estuary. East China Normal University Press, pp 35.

Hu, K., Ding, P., Wang, Z., Yang, S., 2009. A 2D/3D hydrodynamic and sediment transport model for the Yangtze Estuary, China, Journal of Marine Systems, 77 (1–2). ISSN 114–136, 0924–7963. doi:10.1016/j.jmarsys.2008.11.014.

Huang, H., Chen, C., Cowles, G.W., Winant, C.D., Beardsley, R.C., Hedstrom, K.S., Haidvogel, D.B., 2008. FVCOM validation experiments: comparisons with ROMS for three idealized barotropic test problems. Journal of Geophysical Research 113, C07042. doi:10.1029/2007JC004557.

Johns, B., Dube, S., Sinha, P., Mohanty, U., Rao, A., 1982. The simulation of a continuously deforming lateral boundary in problems involving the shallow water equations. Computer and Fluids 10, 105–116.

Jin, N., Tan Z., Li W. and Yu Z., 2003. Siltation issue of Deepwater Channel in Yangtze Estuary, China Harbour, Engineering, 125, No.4 (in Chinese).

Jin, N., Huang, Y., 2005. New progress in estuary regulation techniques in Yangtze Estuary Deepwater Channel Regulation Project. China Harbor Engineering 16, 11–16 (in Chinese).

Jin, N., Zhu, J., 2005. Progresses of Deepway Channel Regulation Project. China Water Transport 7, 52–53 (in Chinese).

Kees, C.E., Akkerman, I., Farthing, M.W., Bazilevs, Y., 2011. A conservative level set method suitable for variable-order approximations and unstructured meshes. Journal of Computational Physics 230, 4536–4558.

Kurzke, M., Weitbrecht, V., and Jirka, G. H., 2002. Laboratory concentration measurements for determination of mass exchange between groin fields and main stream, Proceedings of River Flow 2002, Louvain-la- Neuve, Belgium, 69–76.

Kobayashi, M.H., Pereira, J.M.C., Pereira, J.C.F., 1999. A conservative finite-volume second order-accurate projection method on hybrid unstructured grids. Journal of Computational Physics 150, 40–45.

Lhomme, J., Sayers P., Gouldby B., Samuels P., Wills M., and Mulet-Marti J., 2008. Recent development and application of a rapid flood spreading method, Flood Risk Management – Research and Practice, Proceedings of FLOODrisk 2008, Keble College, Oxford, UK, 15-24.

Le, J., Zhou, H., Guo, Y., 2006. Earlier research and general scheme determination on Yangtze Estuary Deepwater Channel Regulation Project. Port & Waterway Engineering 12, 1–9 (in Chinese).

Liu, J., 2008. Study on morphological evolution and siltation in deep waterway due to channel re-construction in the North Passage, Yangtze Estuary, Doctoral degree thesis of East China Normal University, 38–55 (in Chinese).

Lynch, D., Gray, W., 1980. Finite element simulation of flow in deforming regions. Journal of Computational Physics 36 (2), 135–153. doi:10.1016/0021-9991(80)90180-1.

McCoy, A., Constantinescu, S.G., Weber, L., 2006. Exchange processes in a channel with two vertical emerged obstructions. Flow, Turbulence and Combustion 77, 97–126.

McCoy, A., Constantinescu, S.G., Weber, L., 2007. A numerical investigation of coherent structures and mass exchange processes in channel flow with two lateral submerged groynes, Water Resources Research. VOL. 43, W05445. doi:10.1029/2006WR005267, 2007.

McCoy, A., Constantinescu, S.G., Weber, L., 2008. Numerical investigation of flow hydrodynamics in a channel with a series of groynes. Journal of Hydraulics Engineering 134, 157–172.

Mellor, G.L, Yamada, T., 1982. Development of a turbulence closure model for geophysical fluid problem. Reviews of Geophysical and Space Physics 20, 851–875.

Muto, Y., Baba, Y., and Fujita, I., 2002. Velocity measurements in rectangular embayments attached to a straight open channel, Proceedings of River Flow 2002, Louvain-la-Neuve, Belgium, 1213–1219.

Ouillon, S., Dartus, D., 1997. Three-dimensional computation of flow around groyne. Journal of Hydraulics Engineering 123 (11), 962–970.

Pullen, T., Allsop N.W.H., Bruce T., Kortenhaus A., Schuttrumpf H., and van der Meer, J.W., 2007. EurOtop: Wave Overtopping of Sea Defenses and Related Structures: Assessment Manual (pdf download available from www.overtopping-manual.com).

Pullen, T., Allsop, N.W.H., Bruce T., Kortenhaus A., Schuttrumpf H., and van der Meer, J.W., 2008. EurOtop: Overtopping and methods for assessing discharge, Proceedings of FloodRisk, Oxford, UK.

Pullen, T., Tozer, N., Hawkes, P. and Bruce, T., 2009. A comparison of field and laboratory overtopping measurements with empirical, numerical and probabilistic predictions, Coasts, Marine Structures and Breakwater 2009 Conference, EICC, Scotland, 16-18.

Qi, D., 2003. Numerical modelling research of the optimization of engineering configurations at Deepway Phase II in Changjiang Estuary, Technical report of Shanghai Estuarine and Coastal Science Research Center, 27–31 (in Chinese).

Smagorinsky, J., 1963. General circulation experiments with the primitive equations: I. The basic experiment, Monthly Weather Review 91, 99–164.

Tang, X., Ding, X., Chen, Z., 2006. Large eddy simulations of three-dimensional flows around a spur dike. Tsinghua Science and Technology 11 (1), 117–123.

Uijttewaal, W., 2005. Effects of groyne layout on the flow in groyne fields: Laboratory experiments. Journal of Hydraulics Engineering 131, 782–794.

Uijttewaal, W., Lehmann, D., van Mazijk, A., 2001. Exchange processes between a river and its groyne fields: Model experiments. Journal of Hydraulics Engineering 127, 928–936.

Wu. H., 2006. Saltwater Intrusion in the Changjiang Estuary––Impact of Saltwater Spilling Over, Deep Waterway Project and Winter Monsoon, Doctoral degree thesis of East China Normal University, 88–90 (in Chinese).

Xue, P., Chen, C., Ding, P., Beardsley, R.C., Lin, H., Ge, J., Kong, Y., 2009. Saltwater intrusion into the Changjiang River: A model-guided mechanism study. Journal of Geophysics Research 114, C02006. doi:10.1029/2008JC004831.

Yeo, H., Kang, J., 2008. Flow analysis around a submerged groyne, i. Hohai University, Nanjing, China.

Yossef, M. F. M., 2005. Morphodynamics of rivers with groynes, Ph.D. thesis, Delft Univ. of Technology, Delft, Netherlands.

Yossef, M.F.M., Vriend, H.J., 2011. Flow Details near River Groynes: Experimental Investigation. Journal of Hydraulics Engineering 137, 504–516.

Zhao, L., Chen, C., Vallino, J., Hopkinson, C., Beardsley, R.C., Lin, H., Lerczak, J., 2010. Wetland-estuarine-shelf interactions in the Plum Island Sound and Merrimack River in the Massachusetts coast. Journal of Geophysics Research 115, C10039. doi:10.1029/2009JC006085.

Zheng, L., Chen, C., Liu, H., 2003. A 3-D modeling study of the Satilla River estuarine System. Part I: simulation of flooding/drying processes, Estuaries 26 (3), 651–669.